HMG Advance Access published April 16, 2015

Whole Exome Sequencing Reveals *ZNF408* as a New Gene Associated With Autosomal Recessive Retinitis Pigmentosa with Vitreal Alterations

Almudena Avila-Fernandez[1,2,11], Raquel Perez-Carro[1,2,11], Marta Corton[1,2], Maria Isabel Lopez-Molina[3], Laura Campello[4], Alex Garanto[5,6], Laura Fernadez-Sanchez[4], Lonneke Duijkers[5], Miguel Angel Lopez-Martinez[1,2], Rosa Riveiro-Alvarez[1,2], Luciana Rodrigues Jacy da Silva[1,2,7], Rocío Sanchez-Alcudia[1,2], Esther Martin-Garrido[1,2], Noelia Reyes[1,2], Francisco Garcia-Garcia[8,9], Joaquin Dopazo[8,9,10], Blanca Garcia-Sandoval[3], Rob W. Collin[5,6], Nicolas Cuenca[4], Carmen Ayuso[*,1,2]

[1]Department of Genetics, Instituto de Investigacion Sanitaria-Fundacion Jimenez Diaz University Hospital (IIS-FJD, UAM), Madrid, Spain

[2]Centre for Biomedical Network Research on Rare Diseases (CIBERER), ISCIII, Madrid, Spain

[3]Department of Ophthalmology, IIS-Fundacion Jimenez Diaz University Hospital, Madrid, Spain

[4]Department of Physiology, Genetics and Microbiology, University of Alicante, Alicante, Spain

[5]Department of Human Genetics, Radboud university medical center, 6525 GA Nijmegen, The Netherlands

[6]Radboud Institute for Molecular Life Sciences (RIMLS), Radboud university medical center, 6525 GA Nijmegen, The Netherlands

[7]Universidade de Mogi das Cruzes, São Paulo, Brazil

[8]Computational Genomics Department, Centro de Investigación Príncipe Felipe (CIPF), Valencia, Spain

[9]Bioinformatics in Rare Diseases (BIER), Centro de Investigación Biomédica en Red de Enfermedades Raras (CIBERER), Valencia, Spain

[10]Functional Genomics Node (INB), Valencia, Spain

[11]These authors contributed equally to this work

[*]Corresponding Author: Carmen Ayuso, Head of Research Area, Chief of Clinical Genetics Department, University Hospital Fundación Jiménez Díaz , UAM (IIS-Fundacion Jimenez Diaz), Av. Reyes Católicos Nº 2. Madrid 28040 SPAIN, Phone: ##-34- 609612728, Fax: ##-34 91 550-48-49, E-mail: cayuso@fjd.es

Abstract

Retinitis Pigmentosa (RP) is a group of progressive inherited retinal dystrophies that cause visual impairment as a result of photoreceptor cell death. RP is heterogeneous, both clinically and genetically making difficult to establish precise genotype-phenotype correlations. In a Spanish family with autosomal recessive RP (arRP), homozygosity mapping and whole exome sequencing led to the identification of a homozygous mutation (c.358_359delGT; p.Ala122Leufs*2) in the *ZNF408* gene. A screening performed in 217 additional unrelated families revealed another homozygous mutation (c.1621C>T; p.Arg541Cys) in an isolated RP case. ZNF408 encodes a transcription factor that harbors ten predicted C2H2-type fingers thought to be implicated in DNA binding. To elucidate the ZNF408 role in the retina and the pathogenesis of these mutations we have performed different functional studies. By immunohistochemical analysis in healthy human retina, we identified that ZNF408 is expressed in both cone and rod photoreceptors, in a specific type of amacrine and ganglion cells, and in retinal blood vessels. ZNF408 revealed a cytoplasmic localization and a nuclear distribution in areas corresponding with the euchromatin fraction. Immunolocalization studies showed a partial mislocalization of the p.Arg541Cys mutant protein retaining part of the WT protein in the cytoplasm. Our study demonstrates that *ZNF408*, previously associated with Familial Exudative Vitreoretinopathy (FEVR), is a new gene causing arRP with vitreous condensations supporting the evidence that this protein plays additional functions into the human retina.

Introduction

Retinitis Pigmentosa (RP [MIM number 268000]) is the most common manifestation of inherited retinal dystrophy, with a worldwide prevalence of 1:4,000 approximately (1). It is characterized by a progressive degeneration of rod photoreceptors, leading to night blindness and constriction of the visual field, followed by the degeneration of cone photoreceptors, resulting in a total loss of vision.

There is a large variability in the age of onset, progression, retinal appearance and final visual outcome (2). RP is inherited in all Mendelian forms: autosomal dominant (20% of the cases), autosomal recessive (30%) or X-linked trait (10%). Approximately 40% of patients with RP represent isolated cases; the percentage varies among different populations (3, 4). Non-Mendelian inheritance patterns such as digenic, mitochondrial or *de novo* mutations have been reported, accounting for a small proportion of cases (2).

To date, more than 70 genes have been associated with RP, being heterogeneous, both clinically and genetically. However, mutations in these genes account for the disease in little over half of all patients thus, remaining genes yet to be identified (4, 5). Although the function of some of these genes have been extensively studied, it is difficult to establish a precise genotype-phenotype correlation because mutations in different RP genes can cause overlapping clinical phenotypes (6).

The *ZNF408* gene encodes a zinc finger protein of 720 amino acids that is predicted to harbor ten C2H2-type finger binding domains thought to be implicated in DNA binding.

Recently, in a large Dutch family, a heterozygous missense p.His455Tyr variant in *ZNF408* has been associated to Familial Exudative Vitreoretinopathy (FEVR [MIM number 133780]), a disorder affecting the growth and development of blood vessels in the retina (7).

Interestingly, in this study novel homozygous mutations in the *ZNF408* gene have been identified in two unrelated Spanish families as cause of RP. These findings support the hypothesis that different mutations, either in heterozygous or homozygous state, produce completely different phenotypes and suggest that ZNF408 may play additional roles apart from

its implication in vasculature development. In this context, this is the first time the expression and cellular distribution of ZNF408 have been studied in the human retina.

Results

Selected family and summary of the studies performed

Two affected siblings (II:1 and II:2) of a Spanish family (RP-0322), whose parents came from the same and small geographic region (*Figure 1A*), were diagnosed with autosomal recessive RP (arRP). In order to identify the genetic cause underlying the arRP within the family, first we performed whole genome homozygosity mapping using high resolution SNP-array and further whole-exome sequencing (WES) analysis. A previous genotyping study for the index case (II:2) allowed discarding known mutations associated with arRP. Also, direct Sanger sequencing of the coding exons and flanking intronic sequences of *EYS* did not detect any mutated allele (8).

Genetic Analysis

Homozygosity mapping and Whole-Exome Sequencing (WES) Analysis. Whole genome homozygosity mapping in II:1 and II:2 of RP-0322 family was performed. The two affected siblings shared four homozygous regions ranging from 2.6 to 1.8 Mb (*Table 1*). These regions contain a total of 193 genes, none of which were previously associated with Retinal Dystrophies (RD).

Subsequently, the index case (II:2) of RP-0322 family was analysed by WES. A total of 88,299,239 reads were uniquely mapped to exonic regions with a median of coverage of 59X (mean coverage 69.5X).

After excluding those variants present in non-coding regions and common variants with a minor allele frequency (MAF) <0.005 at dbSNP, 1000 genomes (1000g) or the Exome Variant Server (EVS) databases, we reduced the number of candidate variants underlying RP from 8,133 to 276 (*Table 2*). Assuming an autosomal recessive inheritance pattern and taking into account a very likely common ancestry in the affected family, homozygous variants lying in the previously identified homozygous regions were prioritized (*Table 2*). Also, the expression in human retinal tissues was considered. With this criteria, only one likely pathogenic candidate variant remained, i.e. a frameshift variant in exon 3 of *ZNF408* (NM_024741.2: c.358_359delGT;

p.Ala122Leufs*2) (*Figure 1B*). Due to its implication in vasculature development previously described and its expression in human retina, the *ZNF408* gene was selected as a new candidate gene causing arRP.

Sanger sequencing of the specific region confirmed the presence of this variant identified by WES (*Figure 1A*). This variant was not found in 374 ethnically control alleles nor in 1000g or EVS databases.

Screening of the ZNF408 gene in an arRP Spanish cohort. Following this finding, and to determine the prevalence of the *ZNF408* mutations as a potential cause of arRP, mutation analysis of the *ZNF408* gene was performed by Sanger sequencing in 217 additional Spanish probands affected with sporadic and/or arRP. An additional *ZNF408* variant (c.1621C>T; p.Arg541Cys) was found homozygously in a sporadic case from a consanguineous Spanish RP family (II:2, RP-0976, *Figure 1A*). This variant was not found in a total of 374 healthy control Spanish chromosomes and in SNP databases (1000g and EVS databases). The Arginine residue at position 541 is localized in the seventh of the ten zinc finger domain and is highly conserved across evolution (*Figure 1B,C*).

Two other novel missense variants, p.Gly492Arg and p.Gln583Lys, were identified in heterozygous state in two other arRP patients. Both missense changes were not present in 75 in-house exome datasets. These residues are highly conserved (*Figure 1C*). and *in silico* predictions of the pathogenicity of these two missense variants assessed both of them as deleterious (*Table* 3).

In addition, a Comparative Genomic Hybridization array (aCGH) with an exonic coverage (*Figure S1*) was performed to discard large deletions and copy number variations (CNVs) in the *ZNF408* locus in both patients. No second allele was found in these two patients.

The variants p.Gly492Arg and p.Gln583Lys are highly conserved across the evolution (*Figure 1C*) , rendering it possible that these variants affect ZNF408 protein function but are not responsible for the phenotype in these particular patients.

Ophthalmic examination

The age of onset in all affected individuals (II:1 and II:2, RP-0322 and II:2, RP-0976) was 30, 40 and 17 years, respectively. Night blindness was the first symptom followed by visual field loss and reduction of visual acuity for all patients. At the time of the last ophthalmologic examination, visual fields were symmetrically reduced from 30 to 10 degrees. The best corrected visual acuity (BCVA) ranged from 0.8 to 0.5. Posterior subcapsular cataract was found in all cases. Fundi showed the typical changes of RP with pale optic disc, narrowed vessels, and bone spicule pigmentation (*Figure 2A*). Full-field electroretinogram was nonrecordable or substantially reduced. The ophthalmologic data of the patients are summarized in *Table 4*.

In order to discard any distinctive sign of FEVR an intravenous fluorescein angiography was performed in homozygous (*Figure 2B*) and heterozygous carriers (*Figure S2*). The IVFA for the II:1 (RP-0322) showed classic RP findings and also vitreous alterations in some areas, blurring the visibility of the fundus.. Her affected sibling showed poor pigmentation in a mottled 'salt-and-pepper-like' pattern, especially in the midperiphery. Fluorescein enhancement along the inferior temporal arcades corresponds to retinal pigment epithelium (RPE) atrophy. Also, blurring of the fundus was found in some areas due to vitreous condensation. Similarly to the first family, IVFA of patient II:2 (RP-0976), carrying the missense p.Arg541Cys also showed typical RP fundus findings combined with vitreous condensations that clouds the visibility of the fundus (*Figure 2*).

The asymptomatic heterozygous p.Arg541Cys carriers (III:1 and III:2) from family RP-0976 were examined. No retinal vasculature abnormalities such as an avascular retina, neovascular membranes or tractional retinal detachments were observed in the retinal periphery on fundus, IVFA and OCT (*Figure S2*).

Unfortunately, patients carrying heterozygous p.Gly492Arg and p.Gln583Lys variants were not available for performing additional ophthalmic examination.

ZNF408 is expressed in human retina especially in both cone and rod photoreceptor cells

ZNF408 is abundantly expressed in the human fetal eye as well as in the adult retina, suggesting that ZNF408 has an important role in eye development and visual function (7). However, its

expression at the protein level and its localization in the human retina have never been investigated. To shed light on these aspects, ZNF408 protein expression and its cellular distribution were assessed using Western blot and immunochemistry assays, respectively, on adult healthy human retina as well as in the 661W photoreceptor cell line.

In the human retina, the outer nuclear layer (ONL), ganglion cell layer (GCL) and both outer and inner plexiform layer (OPL and IPL) showed immunoreactivity against ZNF408 antibodies (*Figure 3A*), being strongest at the ONL level.

In this context, ZNF408 immunolabeling at the ONL level presented intense spots of immunoreactivity located around the nuclei of the photoreceptors (*Figure 3A,B,F,G*) and axon terminals (*Figure 3A,B,G*; arrows). Additionally, the ZNF408 immunostaining pattern exhibited a marked expression in a specific subtype of amacrine cell (Figure 3H) and a subtype of ganglion cell of big size, with label in their entire length, including cell body, dendrites and axons (*Figure 3A,B,I*). In addition, ZNF408 immunoreactivity was found in dendrites located in the IPL and in some ganglion cell axons running under the ganglion cell bodies in the nerve fiber layer (NFL) (Figure *3I*).

To verify that the ZNF408 staining was located at the ONL in rod and cones and not in the Müller cells processes, we performed a double immunolabelling with anti-CRALBP antibodies, a specific marker of Müller cells that marks these cells from the outer limiting membrane to the inner limiting membrane, labeling also the RPE (*Figure 3B*). Müller cell bodies were located in the inner most layer in the INL and their external processes pass around the cell bodies of all retinal cells, from the outer to the inner limiting membrane (*Figure 3B* red). Double labeling with anti-CRALBP and anti-ZNF408 antibodies showed no colocalization (*Figure 3B*). Higher magnifications in *Figures 4A-C* (arrowheads) showed absence of this colocalization verifying thus that ZNF408 is located in cell bodies, cytoplasm and myoids of photoreceptor cells but not in Müller cells.

A closer view of the ONL showed that both rods (*Figure 3F arrowheads*) and cones (*Figure 3G*; arrowheads) photoreceptor cells presented ZNF408 immunoreactivity. At the OPL level rod spherules (*Figure 3A,B,G*; arrows) and cone pedicles (double arrows in *Figures 3A,B,G* and *4L*)

were easy to identify. Additionally, a weaker staining was observed in the inner and outer segments (*Figure 3A,G*). To confirm these results, we performed double immunostaining using antibodies raised against recoverin that label cone or rod photoreceptors and some type of bipolar cells, and anti-ZNF408. In this context, it was shown (*Figure 4D-F*) colocalization of anti-ZNF408 and anti-recoverin in both, cone and rod photoreceptors. Immunoreactivity in rod myoids is sharply reduced at the OLM level (arrowheads in *Figures 3A,B,F* and *4A-C*) and only a weak immunostaining was observed in rod and cone outer segments. Double immunolabeling with anti-rhodopsin antibodies, a specific marker for rod outer segments, showed colocalization with the weak anti-ZNF408 immunoreactivity at this level (*Figure 4G-I*). Cone photoreceptor cells exhibited a bright ZNF408 immunoreactivity in its cell bodies, myoids, axons and pedicles while ellipsoids and outer segments showed a lower immunostaining signal, as revealed the double immunolabeling against anti-cone arrestin (*Figure 4J-L*).

As addressed before, ZNF408 is related with FEVR (7). Double immunolabeling using anti-ZNF408 and anti-collagen IV, a specific marker of blood vessels wall, was performed. *Figure 4M-O* showed ZNF408 positive cells into blood vessels, which are presumably endothelial cells (*Figure 4M-O*; insets). Additionally, an immunofluorescence dotted along the cross sections of blood vessels was observed (*Figure 4M-O*, arrows). These results corroborate the relationship found between ZNF408 protein and FEVR patients by Collin and colleagues, supporting thus the role of ZNF408 protein in the development and maintaining of retinal blood vessels.

It is important to remark that the antibody ZNF408 specificity was confirmed by the lack of immunoreactivity in the retina when the antibody was previously preincubated with its blocking peptide (*Figure 3C*).

On the other hand, we performed immunocytochemistry analysis in the mouse retinal photoreceptor-derived 661W cell line. In this context, the ZNF408 immunolabeling exhibited a nuclear and cytoplasmic punctate staining pattern (*Figure 3D,E*). It is important to highlight the ZNF408 staining in nuclei, as expected given that the *ZNF408* gene encodes a transcription factor that harbors ten predicted C2H2-type finger binding domains thought to be implicated in DNA binding (7). In all cases, the staining pattern appeared in the areas of the nucleus

corresponding with the euchromatin fraction (*Figure 3E*). Interestingly, this nuclear distribution was also observed in the human retina as demonstrated in cones and rods (*Figure 3F,G*), neurons in the INL and ganglion cells (*Figure 3A,I*).

The immunoblotting analysis revealed the presence in the human retina and in the 661W cell-line samples of a prominent and specific immunoreactive band with an apparent molecular weight of approximately 67 kDa corresponding to the ZNF408 protein (*Figure 3J*). We confirmed the specificity of the antibody by verifying that preadsorption of the antibody with the immunogenic peptide interferes with the ZNF408 detection. The observed size which was lower than the predicted for the isoform encoded by the canonical *ZNF408* transcript (78.439 kDa) could be the result of a non-uniform binding of the negatively charged SDS to the protein due to its amino acid composition or the presence of a post-translational cleavage of canonical protein, among others.

Partial mislocalization of WT ZNF408 in presence of mutant p.Arg541Cys protein

Constructs of the wild-type (WT) and the p.His455Tyr mutant together result in mislocalization of the WT ZNF408 in the cytoplasm suggesting oligomerization of ZNF408 WT and mutant proteins (7). In order to probe the behavior of our arRP-associated p.Arg541Cys variant, similar ZNF408 WT and mutant cotransfection studies were performed. Constructs expressing N-terminal HA-tagged fusion proteins of WT_ZNF408 or the ZNF408_p.Arg541Cys mutant were generated. The analysis of more than 100 cells by immunocytochemistry of transiently transfected COS-1 cells revealed that localization of WT is exclusively restricted to the nucleus. The p.Arg541Cys mutant ZNF408 also mainly localizes to the nucleus, but occasionally is also present in the cytoplasm of the transfected cells (*Figure 5A,B*). In both cases, the accumulation of both mutants in the cytoplasm were statistically significant. However, the p.Arg541Cys mutant did not show a statistically significant decrease in the amount of cells showing nuclear localization of the ZNF408 protein when compared to the p.His455Tyr mutant. Upon cotransfection analysis of GFP-tagged WT ZNF408 and HA-tagged p.Arg541Cys mutant ZNF408, in those cells where p.Arg541Cys ZNF408 is located in the cytoplasm, it appears to also result in mislocalization of the WT ZNF408 (*Figure 5D*). Although similar observations

were found with the p.His455Tyr mutant, the amount of mislocalized WT ZNF408 protein appears to be less compared to the FEVR-causing p.His455Tyr variant (*Figure 5C,D).*

Discussion

In this study, we combined homozygosity mapping and whole exome sequencing analysis to identify two novel homozygous mutations in *ZNF408* in unrelated Spanish families affected with RP. Furthermore, our functional studies provide evidence for the first association of this gene with inherited Retinal Dystrophy to date.

ZNF408 belongs to a large family of transcription factors characterized by an N-terminal a set domain and tandem C-terminal C2H2-type zinc fingers. This gene is highly expressed in human adult and fetal retinal tissues, as was shown by RT-PCR analysis (7), suggesting that *ZNF408* could have an important role in retina development and homeostasis.

A heterozygous mutation in ZNF408 has been previously described as cause of FEVR. FEVR is a rare, autosomal dominant inherited disorder characterized by an incomplete vascularization of the peripheral retina and/or retinal blood vessel differentiation.

However, the two RP families described herein did not show any evident sign of FEVR. Interestingly all affected members of both families presented some vitreous alterations but, the ZNF408-linked RP phenotype of our individuals is completely different from that of FEVR and thus represents a different clinical form caused by mutations in *ZNF408*.

Previous studies have been described posterior vitreous detachment and other vitreous alterations, including fibrillary degenerations, floaters, cottonball-like condensations, non-pigmentary and pigmentary particulation in RP patients (9-11). In our patients, the density of the vitreal alterations is higher to the previously described, blurring the fundus resembling the vitreoretinal dystrophies although the morphology is not exactly veils. Therefore, the homozygous mutations described seem to cause a consistent typical RP phenotype with minor vitreous abnormalities other than those found in FEVR patients.

Strikingly, in the RP-0322 family, we have found a homozygous frameshift mutation that it is expected to truncate the ZNF408 protein at its N-terminal, and thus predicted to result in a complete loss-of-function of ZNF408. The identification of a homozygous likely pathogenic

missense variant in a second family strongly supports the implication of *ZNF408* in retinal degeneration. Our data suggest that ZNF408 may have essential functions in maintenance of retinal homeostasis, in addition to its role in vasculature development.

Since FEVR is inherited as an autosomal dominant manner and it is known that asymptomatic FEVR patients frequently have very early manifestation of the vitreoretinal findings on angiography (12), an exhaustive ophthalmic examination was performed to exclude any symptom of FEVR in heterozygous carriers of the missense variants found in this study. However, no vascular alterations were observed in the examined asymptomatic individuals.

It is intriguing how different mutations in *ZNF408* could cause distinctive phenotypes of retinal disease with clearly different pathogenic mechanisms and also unequivocal inheritance patterns, such as adFEVR and arRP.

As previously described, the FEVR-associated p.His455Tyr variant could act as dominant-negative mutation. However, although the partial retention of the WT_ZNF408 by the ZNF408_p.Arg541Cys mutant was shown, this is not enough to produce a dominant-negative effect suggesting different mutational mechanisms for these two variants. This hypothesis is also strongly supported by the absence of phenotypic alterations in heterozygous carriers of the p.Arg541Cys mutation, i.e. neither displaying features of arRP nor adFEVR.

Zinc fingers are elements for DNA binding found in a high number of proteins which participate in a wide variety of cellular activities (13). The greater the number of finger domains, the higher versatility and the more fingers with specific affinity for different ligands in specific classes of proteins (14, 15). ZNF408 comprises ten of such domains that could have different and still unknown cellular functions in several parts of the organism. The presence of mutations in these different domains suggests these changes are altering the interaction of ZNF408 with specific targets, thereby resulting in the dysregulation of different target genes and subsequently are underlying either FEVR or RP.

Although further studies are mandatory to elucidate the role of ZNF408 in the human retina, it is also important to highlight the ZNF408 staining pattern localizes in the dark areas of the nucleus corresponding with the euchromatin fraction supporting the hypothesis that *ZNF408* encodes a

transcription factor widely expressed in the human retina. Mutations in other genes encoding transcription factors, such as the photoreceptor-specific nuclear receptor subfamily 2 group E member 3 (*NR2E3*) gene, which plays a critical role in the photoreceptor differentiation, have been associated with a variety of retinal dystrophies, such as RP, Goldman-Favre disease or Enhanced S-cone syndrome, and can display different clinical features and patterns of inheritance, including autosomal-dominant and autosomal recessive (16-19).

Further studies on the identification of the transcriptional targets of ZNF408 could help us to highlight new genes implicated for retinal development that could be good candidates for RD. Here, in order to identify the disease-causing gene in a Spanish family diagnosed with autosomal recessive RP (arRP), we have performed a combined approach including whole homozygosity mapping followed by a whole exome sequencing analysis (WES). The study revealed the presence of two novel different mutations in the *ZNF408* gene in two unrelated arRP Spanish families and thereby expanding the spectrum of *ZNF408* mutations to be associated with a new phenotype consisting of RP with vitreous condensations.

Materials and Methods

Patient Recruitment

Patients diagnosed with RP were recruited from the Biobank of the Fundación Jiménez Díaz Hospital (Madrid, Spain). Diagnostic criteria of RP included night blindness and/or peripheral visual loss, with visual field loss and poor visual acuity in advanced stages of the disease. A commercial arRP genotyping microarray v2.0 (AsperBiotech, Tartu, Estonia) was used in the index cases to discard known mutations (20). A total of 218 unrelated Spanish families with autosomal recessive or sporadic RP were selected. Informed consent was obtained from all patients and family members or their legal guardians involved in the study. All procedures were reviewed and approved by the Ethics Committee of the Hospital and adhered to the tenets of the Declaration of Helsinki (Fortaleza 2013).

One hundred and eighty seven unrelated individuals of Spanish origin without RP family history were screened as controls to evaluate the frequency of the missense mutation found in this study.

Peripheral blood samples from all participating individuals were collected in EDTA tubes. Genomic DNA was extracted with an automated DNA extractor (model BioRobotEZ1; QIAGEN, Hilden, Germany) following the manufacturer's instructions.

Genetic Analysis

Homozygosity mapping

A whole-genome homozygosity mapping was performed using Affymetrix 6.0 genotyping arrays (Affymetrix, Inc, Santa Clara, CA). Arrays were processed according to manufacturer's protocols by the Spanish Center for Genotyping (CEGEN, Santiago de Compostela, Spain). Homozygosity regions were calculated using the Linkage Disequilibrium–Hidden Markov Model algorithm (21) through the dCHIP software (22). Regions with a size >1Mb were considered candidate regions to harbour the genetic defect.

Next Generation Sequencing (NGS)

Whole-exome sequencing (WES) analysis was performed by the Spanish Centre for Genome Analysis (CNAG, Barcelona, Spain). The SureSelect Human All Exon Version 4 kit (Agilent Technologies, Santa Clara, CA, USA) was used for in-solution enrichment of coding exons and flanking intronic sequences following the manufacturer's standard protocol. Sequencing was done with an Illumina HiSeq2000 sequencing platform (Illumina) generating paired-end reads up to 100 cycles.

Base calling and quality control were performed using the Illumina RTA sequence analysis pipeline. Bioinformatic analysis of the sequencing data was done by the Bioinformatic Platform for Rare Diseases (CIBERER-BIER, http://www.ciberer.es/bier/), using standard tools for quality control, sequence alignment, and variant calling in combination with our own in-house scripts including that of single nucleotide variants (SNVs) and small indels (23).

Sanger sequencing analysis

Bidirectional automatic sequencing was performed in order to confirm and segregate the obtained results by whole exome sequencing, also to screen the *ZNF408* gene in 217 additional arRP families, and to determine the frequency of one of the missense variations in the control population. Exons and exon-intron boundaries of the *ZNF408* gene (NM_024741.2) were

analyzed using 8 oligonucleotide primers pairs designed using Primer3 software. Sequences and annealing temperatures are available on request. The PCR products were enzymatically purified with ExoSAP-it (USB, Affymetrix) and sequenced using Big Dye Terminator Cycle Sequencing Kit version 1.1 (Applied Biosystems, Carlsbad, CA). The PCR products were resolved on an automated sequencer (ABI 3130xl Genetic Analyzer, Applied Biosystems).

Sequencing results were analyzed by using Staden Package 1.7.0 software by assembling and visualizing the aligned sequences of the exons.

Prediction of the pathogenic effect of the variants

Pathogenicity of this variant was firstly assessed by co-segregation with the disease in the family, by its absence in a total of 374 healthy control Spanish chromosomes and in SNP databases (1000g and EVS databases) and by bioinformatic prediction tools (SIFT, Polyphen2 and align-GVGD) which classified this variant as most likely damaging and by the amino acid conservation across 5 orthologs of the ZNF408 protein belonging to different evolutionary branches. The Clustal Omega tool and the Jalview Alignment Editor program were used to analyze the multiple sequence alignments.

Comparative Genomic Hybridization array (aCGH)

The custom aCGH 8X60k using Agilent SurePrint G3 CGH was designed using the Agilent eArray website (https://earray.chem.agilent.com/earray/) with an average distribution of 1 probe per 150pb in the *ZNF508* gene.

Briefly, genomic DNA (200ŋg) from the patient and from a sex-matched control were digested by *Alu* I and *Rsa* I restriction enzymes for 2 h at 37°C and the digested products were labeled with Cy3-dUTP and Cy5-dUTP fluorochromes using the Sure Tag DNA Labeling Kit (Agilent Technologies). The labeled products were purified, hybridized and washed according to Agilent protocols. The slide was scanned on a SureScan G4900DA scanner (Agilent Technologies), and the resulting TIFF images were converted by the image conversion Feature Extraction software (Agilent Technologies). Results were analyzed by Agilent CytoGenomics software v.2.7 using default analysis method – CGH v2 with the ADM-2 aberration algorithm.

Ophthalmic examination

Ophthalmic examinations were performed for all patients with mutations in *ZNF408* and the available heterozygous carriers. The evaluation included visual acuity, intraocular pressure, ocular motility, pupillary reaction, biomicroscopic slit lamp examination and dilated fundus examination. Visual function was evaluated by static perimetry and Ganzfeld electroretinography according to the ISCEV (International Society for Clinical Electrophysiology of Vision) (24). An intravenous fluorescein angiography (IVFA) was performed.

Immunohistochemistry

The ZNF408 localization pattern was determined in cryo-fixed healthy adult human retina sections. They were immunostained at room temperature overnight with rabbit polyclonal antibodies to human ZNF408 from Santa Cruz Biotechnology (Santa Cruz, CA, USA; Catalog No. sc-134190) diluted at 1:50 in 0.1 M sodium phosphate buffer (pH 7.4), 0.5% Triton X-100 in the presence or absence of blocking peptide (20:1 peptide: antibody ratio; LifeTein South Plainfield NJ, USA). Double immunocytochemistry with ZNF408 were performed using it in combination with: monoclonal mouse anti-rhodopsin (Millipore Temecula, CA, USA), goat anti–recoverin (Santa Cruz Biotechnology Inc. TX, USA), goat anti-colagen IV (Millopore Temecula, CA, USA) and monoclonal mouse anti-cone arrestin (Dr. MacLeish, Morehouse School of Medicine; Atlanta, GA, USA) (25, 26). In addition, the 661W photoreceptor cell-line was also probed with the ZNF408 antibodies.

Furthermore, ZNF408 protein expression was assessed using Western blotting on adult healthy human retinas as well as in the 661W photoreceptor cell-line. Briefly, proteins were extracted and subjected to immunoblotting analysis. Proteins (40 μg/lane) were resolved by SDS-PAGE on 4–20% polyacrylamide-gradient gels and electrotransferred to Hybond-P PVDF membranes (GE Healthcare, Buckinghamshire, UK). These were probed at 4 °C overnight with the same ZNF408 antibodies used in immunocytochemistry assays at a 1:100 dilution in 25 mM Tris (pH 8.0), 150 mM NaCl, 2.7 mM KCl (TBS) in the presence or absence of blocking peptide (10:1 peptide: antibody ratio; LifeTein South Plainfield NJ, USA), or with mouse monoclonal

antibodies to rabbit muscle GAPDH at a 1:1,000 dilution (Millipore, Temecula, CA, USA; Catalog No. MAB374). Thereafter, the membranes were incubated at room temperature for 1 h with horseradish peroxidase-conjugated goat anti-rabbit or goat anti-mouse (Pierce, Rockford, IL, USA) IgG at a 1:20,000 dilution. Detection was performed by enhanced chemiluminescence using the SuperSignal West Dura system (Pierce).

Transfection of COS-1 Cells

Constructs expressing HA-tagged or eCFP-tagged WT and mutant ZNF408 were designed using the mammalian expression vector pcDNA3-HA/DEST or pcDNA3-eCFP/DEST, both driven by a cytomegalovirus (CMV) promoter.

COS-1 cells where transiently transfected using Effectene (Qiagen) according to the manufacturer´s instructions. In both cases, unpaired Student's t-test as well as Mann-Whitney analyses were used to determine if there were statistically significant differences. Images were obtained with a Zeiss AxioImager Z1 upright fluorescent microscope and processed with a Zeiss ApoTome slider module. All experiments were performed in duplicate (7).

Acknowledgments

We would like to thank to FJD-Biobanco (RD09/0076/00101), Services of Genetics and Ophthalmology IIS-Fundacion Jimenez Diaz, (Madrid). CIBER-ER (06/07/0036), FIS (PI013/00226), Ministry of Economy and Competitiveness-FEDER (BFU2012-36845), and RETICS RD12/0034/0010), Miguel Servet CP/03256 (ISCIII), ONCE & Fundaluce for their support and to Spanish Center for Genotyping (CEGEN, Santiago de Compostela, Spain) for his contributions to this work. PC is supported by Fundación Conchita Rábago (FCR). dS is supported by CAPES Foundation, Ministry of Education of Brazil.

This work is also supported by grants BIO2011-27069 from the Spanish Ministry of Economy and Competitiveness, and PROMETEOII/2014/025 from the Conselleria de Educacio of the Valencia Community.

Conflict of Interest Statement

The authors have no conflicts of interest to declare.

References

1. Ayuso, C. and Millan, J.M. (2010) Retinitis pigmentosa and allied conditions today: a paradigm of translational research. *Genome Med,* **2,** 34.
2. Hartong, D.T., Berson, E.L. and Dryja, T.P. (2006) Retinitis pigmentosa. *Lancet,* **368,** 1795-809.
3. Ayuso, C., Garcia-Sandoval, B., Najera, C., Valverde, D., Carballo, M. and Antinolo, G. (1995) Retinitis pigmentosa in Spain. The Spanish Multicentric and Multidisciplinary Group for Research into Retinitis Pigmentosa. *Clin. Genet,* **48,** 120-2.
4. den Hollander, A.I., Black, A., Bennett, J. and Cremers, F.P. (2010) Lighting a candle in the dark: advances in genetics and gene therapy of recessive retinal dystrophies. *J. Clin. Invest,* **120,** 3042-53.
5. Wright, A.F., Chakarova, C.F., Abd El-Aziz, M.M. and Bhattacharya, S.S. (2010) Photoreceptor degeneration: genetic and mechanistic dissection of a complex trait. *Nat. Rev. Genet,* **11,** 273-84.
6. Berger, W., Kloeckener-Gruissem, B. and Neidhardt, J. (2012) The molecular basis of human retinal and vitreoretinal diseases. *Prog. Retin. Eye Res,* **29,** 335-75.
7. Collin, R.W., Nikopoulos, K., Dona, M., Gilissen, C., Hoischen, A., Boonstra, F.N., Poulter, J.A., Kondo, H., Berger, W., Toomes, C. *et al.* (2013) ZNF408 is mutated in familial exudative vitreoretinopathy and is crucial for the development of zebrafish retinal vasculature. *Proc. Natl. Acad. Sci. U S A,* **110,** 9856-61.
8. Barragan, I., Borrego, S., Pieras, J.I., Gonzalez-del Pozo, M., Santoyo, J., Ayuso, C., Baiget, M., Millan, J.M., Mena, M., Abd El-Aziz, M.M. *et al.* (2010) Mutation spectrum of EYS in Spanish patients with autosomal recessive retinitis pigmentosa. *Hum. Mutat,* **31,** E1772-800.
9. Hikichi, T., Akiba, J. and Trempe, C.L. (1995) Prevalence of posterior vitreous detachment in retinitis pigmentosa. *Ophthalmic Surg,* **26,** 34-8.

10. Vingolo, E.M., Giusti, C., Forte, R. and Onori, P. (1996) Vitreal alterations in retinitis pigmentosa: biomicroscopic appearance and statistical evaluation. *Ophthalmologica,* **210,** 104-7.

11. Sudarshan, A.P. (1999) Vitreous change in retinitis pigmentosa. *Ophthalmology,* **106,** 210.

12. Kashani, A.H., Learned, D., Nudleman, E., Drenser, K.A., Capone, A. and Trese, M.T. (2014) High prevalence of peripheral retinal vascular anomalies in family members of patients with familial exudative vitreoretinopathy. *Ophthalmology,* **121,** 262-8.

13. Pavletich, N.P. and Pabo, C.O. (1993) Crystal structure of a five-finger GLI-DNA complex: new perspectives on zinc fingers. *Science,* **261,** 1701-7.

14. Morgan, B., Sun, L., Avitahl, N., Andrikopoulos, K., Ikeda, T., Gonzales, E., Wu, P., Neben, S. and Georgopoulos, K. (1997) Aiolos, a lymphoid restricted transcription factor that interacts with Ikaros to regulate lymphocyte differentiation. *EMBO J,* **16,** 2004-13.

15. Tsai, R.Y. and Reed, R.R. (1998) Identification of DNA recognition sequences and protein interaction domains of the multiple-Zn-finger protein Roaz. *Mol. Cell Biol,* **18,** 6447-56.

16. Escher, P., Gouras, P., Roduit, R., Tiab, L., Bolay, S., Delarive, T., Chen, S., Tsai, C.C., Hayashi, M., Zernant, J. *et al.* (2009) Mutations in NR2E3 can cause dominant or recessive retinal degenerations in the same family. *Hum. Mutat,* **30,** 342-51.

17. Pachydaki, S.I., Klaver, C.C., Barbazetto, I.A., Roy, M.S., Gouras, P., Allikmets, R. and Yannuzzi, L.A. (2009) Phenotypic features of patients with NR2E3 mutations. *Arch. Ophthalmol,* **127,** 71-5.

18. Kanda, A. and Swaroop, A. (2009) A comprehensive analysis of sequence variants and putative disease-causing mutations in photoreceptor-specific nuclear receptor NR2E3. *Mol. Vis,* **15,** 2174-84.

19. Yang, Y., Zhang, X., Chen, L.J., Chiang, S.W., Tam, P.O., Lai, T.Y., Chan, C.K., Wang, N., Lam, D.S. and Pang, C.P. (2010) Association of NR2E3 but not NRL mutations

with retinitis pigmentosa in the Chinese population. *Invest Ophthalmol. Vis. Sci*, **51,** 2229-35.

20. Avila-Fernandez, A., Cantalapiedra, D., Aller, E., Vallespin, E., Aguirre-Lamban, J., Blanco-Kelly, F., Corton, M., Riveiro-Alvarez, R., Allikmets, R., Trujillo-Tiebas, M.J. *et al.* (2010) Mutation analysis of 272 Spanish families affected by autosomal recessive retinitis pigmentosa using a genotyping microarray. *Mol. Vis*, **16,** 2550-8.

21. Beroukhim, R., Lin, M., Park, Y., Hao, K., Zhao, X., Garraway, L.A., Fox, E.A., Hochberg, E.P., Mellinghoff, I.K., Hofer, M.D. *et al.* (2006) Inferring loss-of-heterozygosity from unpaired tumors using high-density oligonucleotide SNP arrays. *PLoS Comput. Biol*, **2,** e41.

22. Lin, M., Wei, L.J., Sellers, W.R., Lieberfarb, M., Wong, W.H. and Li, C. (2004) dChipSNP: significance curve and clustering of SNP-array-based loss-of-heterozygosity data. *Bioinformatics*, **20,** 1233-40.

23. Aleman, A., Garcia-Garcia, F., Salavert, F., Medina, I. and Dopazo, J. (2014) A web-based interactive framework to assist in the prioritization of disease candidate genes in whole-exome sequencing studies. *Nucleic Acids Res*, **42,** W88-93.

24. Marmor, M.F., Fulton, A.B., Holder, G.E., Miyake, Y., Brigell, M. and Bach, M. (2009) ISCEV Standard for full-field clinical electroretinography (2008 update). *Doc. Ophthalmol*, **118,** 69-77.

25. Martínez-Navarrete, G., Angulo, A., Martín-Nieto, J. and Cuenca, N. (2008) Gradual morphogenesis of retinal neurons in the peripheral retinal margin of adult monkeys and humans. *J. Comp Neurol.* , **511,** 557-80.

26. Fernandez-Bueno, I., Fernández-Sánchez, L., Gayoso, M., García-Gutierrez, M., Pastor, J. and Cuenca, N. (2012) Time course modifications in organotypic culture of human neuroretina. *Exp. Eye Res.*, **104,** 26-38.

Figure Legends

***Figure 1*. *A*.** Pedigrees of the two Spanish studied families with ZNF408 mutations. The index case is indicated with an arrow. Sanger sequencing confirms the mutations identified by WES and reveals their complete cosegregation with the disease. The chromatograms of a control and a homozygous individual with mutations are depicted for each variant (blue line). ***B*.** Schematic overview of ZNF408 taken and modified from Collin *et al*., The mutation previously associated with FEVR is shown in black. The mutations identified in this study and associated with RP are shown in red. ***C*.** Cross-species comparison of the region of ZNF408 indicates that the identified missense mutations affect a highly-conserved residues (red box).

***Figure 2*. Phenotype of affected individuals with mutations in the *ZNF408* gene. *A*.** Spectrum of fundus findings in different individuals. Funduscopy of three patients (II.1 and II.2 of the RP-0322 family and II.2 for the RP-0976 family) shows pale optic disc, attenuation of retinal vessels and bone spicule pigmentation. For the II.2 of the RP-0976 family it is also shown spotty pigmentation and peripapillary atrophy. Macular preservation is observed in all cases. ***B*.** Intravenous Fluorescein Angiography (IVFA) of the patients. For the patient II.1 of the RP-0322 the IVFA shows vitreous alterations blurring fundus in some areas (red arrows). The IVFA for the patient II.2 (RP-0322) shows fluorescein enhancement along the inferior arcades (blue arrow), poor pigmentation in mottled pattern in midperiphery and some areas with vitreous condensations (red arrows). For the individual II.2 of the RP-0976 family the IVFA shows typical RP fundus findings and also vitreous condensations blurring of the fundus in some areas (red arrows). ***C*.** Spectrum of optical coherence tomography (OCT) imaging in different individuals.

***Figure 3*. Immunocytochemistry assays in cryofixed human retina sections and in the 661W photoreceptor cell-line. *A-C,F-H*.** Human retina immunolabeled with antibody against ZNF408 (green) and CRALBP (red). Nuclei are labelled with TO-PRO (blue). (*A,B*) ZNF408 distribution in the ONL, OPL, IPL and GCL. (*B*) Double immunolabeling against CRALBP and ZNF408 antibodies showed no colocalization with Müller cells. (*C*) No immunofluorescence was detected in section using pre-adsorption with the blocking peptide. (*F-G*) High

magnification of photoreceptors showing immunoreactivity in both rods (*F*) and cones (arrowheads) (*G*). ZNF408 is expressed in cell bodies of some type of amacrine (*H*) and ganglion (*I*) cells and its dendrites in the IPL (*A,B,H,I*). Arrows in *A,B,G* indicates spherules of rods while double arrows in *A,B,G* indicates pedicles of cones. Arrowheads in *A,B,G* show ZNF408 immunolabeling at the border of the OLM. Arrows in *F* indicated the rod myoid and cell body.. (*D, E*) Nuclear and cytoplasmic ZNF408 immunoreactivity in the 661W photoreceptor cell-line. Note the ZNF408 localization in the less condensed chromatin areas. (*J*) Immunoblotting analysis of ZNF408 protein. Human retina (from two different individual, HR1 and HR2) and 661W photoreceptor cell-line samples expressed strongly immunoreactive bands detected with ZNF408 or GAPDH antibodies (arrowheads). Protein molecular weight markers are given to the left. ZNF408 staining (peptide -) was specifically abolished when the ZNF408 antibody was preincubated with its immunogen peptide (peptide +). Scale bar *A,B,C,D,E,G,H*=20um, F=10um.

Figure 4. **Immunocolocalization of ZNF408 in cryostat sections of human retina**. Double immunolabeling of ZNF408 with antibodies against CRALBP, a specific marker for Müller cells and RPE (*A,B,C*); recoverin that labels cone and rod photoreceptors (*D,E,F*); rhodopsin, a marker for rod outer segments, (*G,H,I*) and cone arrestin that labels cone photoreceptors (*J,K,L*). Blood retinal vessels were labeled with anti-Collagen IV (*M,N,O*). No colocalization of ZNF408 and Müller cells were found in the ONL (*A-C*, arrowheads). Photoreceptor cells labeled with recoverin antibody showed colocalization with ZNF408 in both cones and rods (*D-F*). ZNF408 showed a weak immunolabeling in rod outer segments labeled with antibodies against rhodopsin (*G-I*). In addition, the double immunostaining with antibodies against arrestin showed a strong colocalization of ZNF408 in cones where it was located on cell bodies, axons and pedicles (double arrowheads), myoids and elipsoids (arrows), as well as a weak immunoreactivity was observed in the outer segments (arrowheads) (*J-L*). Antibodies against collagen IV immunolabeled the retinal blood vessels wall (*N-O*). ZNF408 immunopositive cells were present presumably in endothelial cells of the blood vessels (*M-O*, square), as well as

immunoreactive spots were found along blood vessels in horizontal sections (*M-O*, arrows). Scale bar = 20um.

Figure 5. **Immunocytochemical analysis.** ***A.*** COS-1 cells transiently transfected with constructs encoding HA-tagged WT and mutant (p.His455Tyr, p.Arg541Cys) ZNF408 proteins. DAPI stains cell nuclei (top), whereas the anti-HA antibody stains the ZNF408 fusion proteins (middle). Merged pictures are shown on the bottom. Representative examples are shown for each transfection, indicating full nuclear localization for the WT, but with a partial cytoplasmic localization of the p.His455Tyr and p.Arg541Cys mutant ZNF408 proteins. ***B***. Quantification by fluorescence microscopy. *Significant differences ($p<0.0001$). ***C-D*** Cotransfection analysis of WT and p.His455Tyr and p.Arg541Cys mutant ZNF408 proteins respectively DAPI stains cell nuclei (left), GFP stains ZNF408 WT and anti-HA stains ZNF408 mutants (middle) and on the right the merge pictures are showed.

Ranking	Chr	Start position	End position	Size (Mb)	No. Genes
1	11	44657924	47217647	2.6	59
2	1	146198340	148529079	2.3	56
3	7	116046131	118194089	2.1	17
4	15	38922698	40687683	1.8	61

Table 1. **Homozygous regions shared by the two affected members of the RP-0322 family.**

Listed are homozygous regions > 1 Mb, sorted by size, the start and the end position by hg19 of the regions, the size and the number of genes encompassed each regions. Chr: chromosome; Mb: megabases; No: Number.

Table 2. **WES findings**. Overview of the number of the high-confident variants present, after applying all quality filters, in the index case (II.2) of the RP-0322.

WES finding	**No. Variants**
Total	8133
Potentially functional variants	7570
Heterozygosis	3865
Homozygosis	3705
Effect	7570
Non-synonymous SNV	7131
Splicing	62
Stop-gain SNV	55
Stop-loss SNV	28
Frameshift	187
In-frame	107
MAF<0,005	276
Heterozygosis	150
Homozygosis	126
Variants in LOH	2
Splicing	1
Frameshift	1

***Table 3*. Pathogenicity assessment of *ZNF408* missense changes.** Assessment of pathogenicity for the *ZNF408* missense changes. For Align GVGD, class C65 and C45 represent the highest and moderate, respectively, likelihood of a change to be pathogenic.

Nucleotide change	**Amino acid change**	**Frequency in ethnically matched control alleles**	**Predictions of pathogenicity**		
			SIFT	**Polyphen2**	**Align GVGD**
c.1474G>A	p.Gly492Arg	0/150	Deleterious	Possibly damaging	Class C65
c.1621C>T	p.Arg541Cys	0/374	Deleterious	Possibly damaging	Class C65
c.1747C>A	p.Gln583Lys	0/150	Deleterious	Probably damaging	Class C45

Table 4. **Clinical features of patients with mutations in the *ZNF408* gene.** ID, identification; YR, years; BCVA, best corrected visual acuity, RE, right eye; LE, left eye; ERG, electroretinogram; IVFA, intravenous fluorescein angiography; OCT, optical coherence tomography; NB, night blindness; VA visual acuity; RPE, retinal pigment epithelium; NCD, no clinical data.

Family	**Patient ID**	**Genotype**		**First symptoms and course**	**Age at diagnosis (yr)**	**Age of Ophthalmic Evaluation (yr)**	**BCVA RE/LE**	**Visual Field RE/LE**	**ERG**	**Fundus aspect**	**IVFA**	**OCT**	**Additional findings**
		Gene	**Mutations Allele1/Allele2**										
RP-0322	II:1	*ZNF408*	p.Ala122Leufs*2/ p.Ala122Leufs*2	NB (30yr), field constriction and progressive loss of VA	52	69	0.5/0.8	Restricted to 10º central field	No register	Pale optic disc, narrow vessels, moderate bone spicule pigmentation and RPE atrophy in mid periphery and macular preservation	RP findings and vitreous alterations blurring fundus in some areas	No liquid, perifoveal thinning, incipient epiretinal membrane	Photophobia Posterior subcapsular cataract

	II:2	*ZNF408*	p.Ala122Leufs*2/ p.Ala122Leufs*2	NB (40yr), field constriction and progressive loss of VA	50	67	0.6/0.5	Restricted in superior and temporal hemifield/ Restricted to 30º central field inferonasally	Rods abolished Mixed, cones and flicker diminished	Normal optic disc, mildly attenuated vessels and poor pigmentation in lower hemiretina, macular preservation	Poor pigmentation in mottled pattern specially in midperiphery. Fluorescein enhancement along the inferior temporal arcades. Blurring of the fundus due to vitreous condensation	Normal morphology ,no cysts, incipient epiretinal membrane LE	Photophobia Posterior subcapsular cataract
RP-0976	II:2	*ZNF408*	p.Arg541Cys/p.Arg541Cys	NB, field constriction (17yr) and progressive loss of VA (36yr)	20	50	0.8/0.9	Restricted to 10º central field	NCD	Pale optic disc, peripapillary atrophy, vessel attenuation, both spotty and spicule pigmentation midperiphery, atrophy of the RPE and macular	Typical RP fundus findings combined with vitreous condensations make difficult the visibility of the fundus	Normal morphology in the fovea, no cysts, atrophy in the periphery	Photosensitivity Posterior subcapsular cataract High myopia

reservation

A

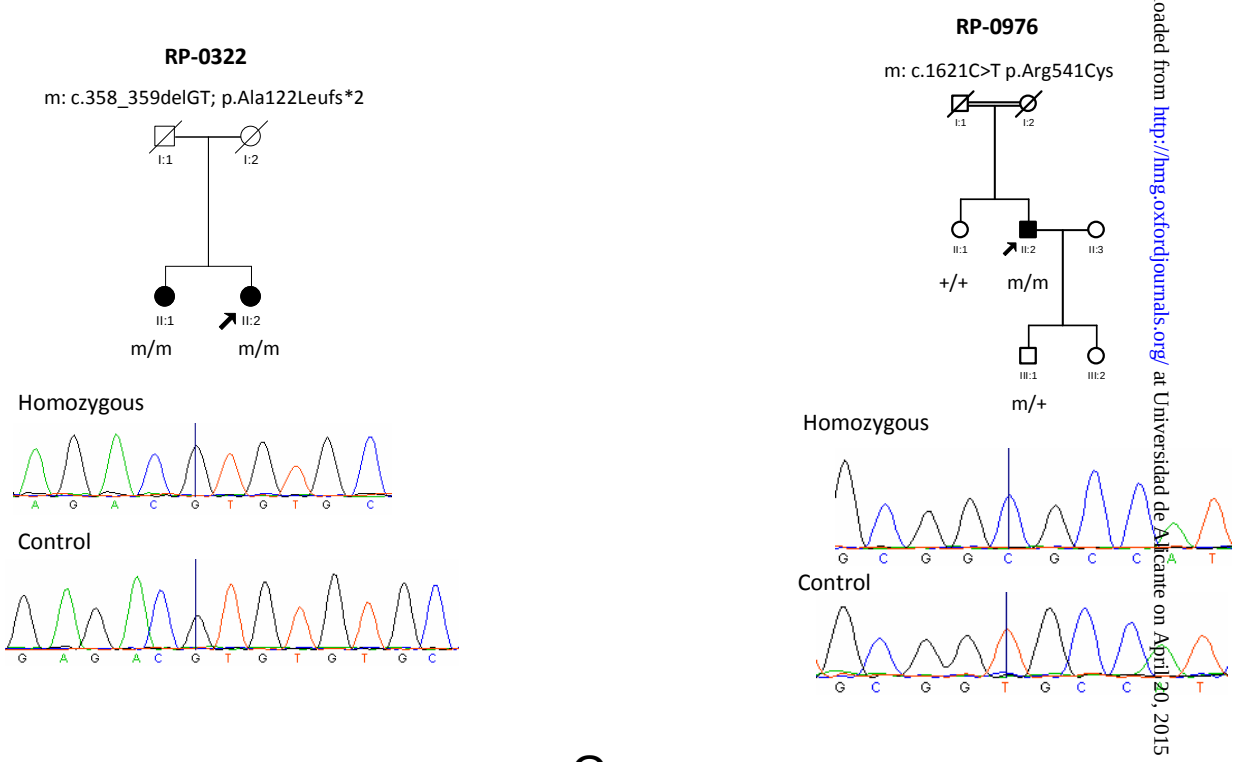

B

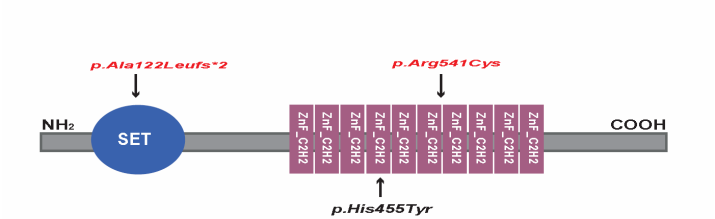

C

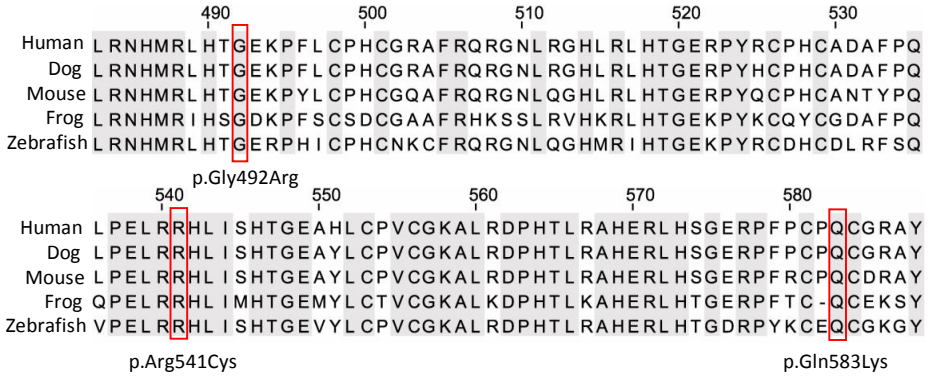

A. Fundus

RP-0322
II.1

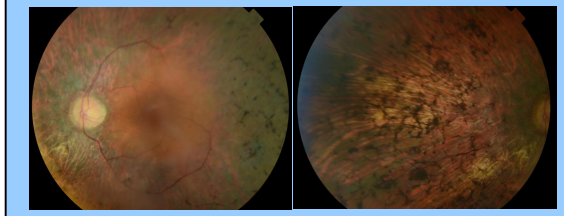

II.2

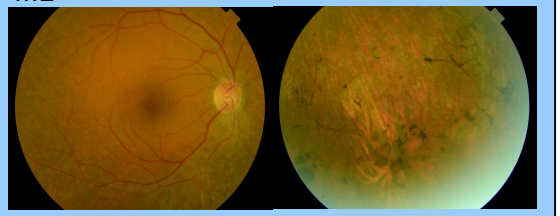

RP-0976
II.2

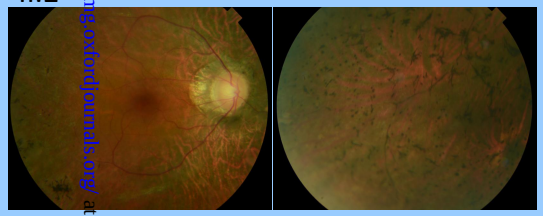

B. IVFA

RP-0322
II.1

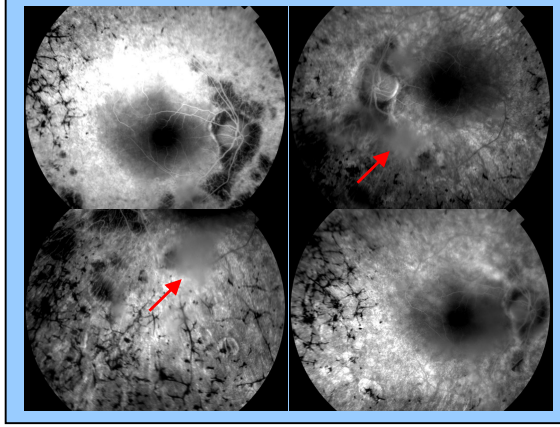

II.2

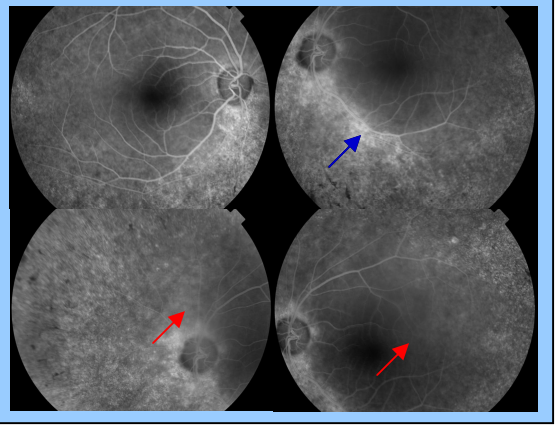

RP-0976
II.2

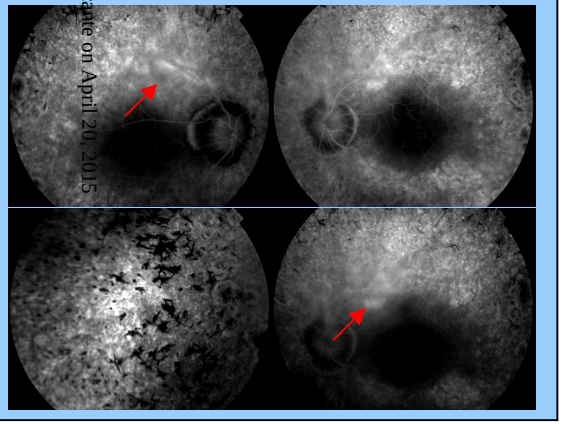

C. OCT

RP-0322
II.1

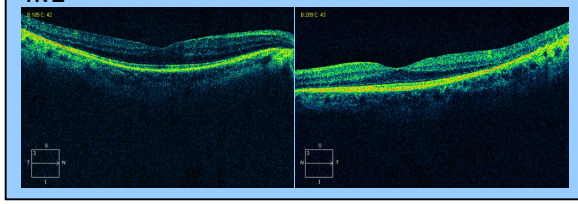

II.2

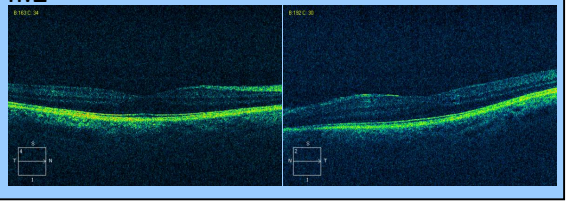

RP-0976
II.2